Journal of Nuclear Materials 145–147 (1987) 15–25
North-Holland, Amsterdam



# REVIEW OF MARFE PHENOMENA IN TOKAMAKS *

B. LIPSCHULTZ

*Plasma Fusion Center, MIT, Cambridge, MA, 02139, USA*

Key words: scrape-off layer, radiating edge, H-mode, impurity generation

This paper presents a review of MARFEs and detached plasmas. A MARFE is a toroidally symmetric tokamak phenomenon occuring at minor radii near the plasma boundary, defined by a limiter or magnetic separatrix. The MARFE poloidal width is approximately 30° in extent at the smaller major radius edge of the plasma. It is characterized by greatly increased radiation, high ion densities and density fluctuations, and relatively low electron temperature. These changes in the edge plasma are consistent with the MARFE being the manifestation of a thermal instability. MARFEs tend to occur in most tokamaks at similar values of $\rho = \bar{n}_e/\kappa J$, a fraction of the density disruption limit. A related phenomenon, the detached plasma, is different in that the boundary layer radiation emission is poloidally symmetric. The radiated power, in this case, is approximately equal to the input power, thereby reducing power flows to the limiter to negligible values. A review of experimental data and theoretical treatments of MARFEs and detached plasmas are provided herein. The relationship between boundary layer parameter scalings, the MARFE threshold and the density limit is explored.

## 1. Introduction

There is increasing recognition that the plasma in the scrapeoff layer (SOL), $r \geq a$, plays an important part in improving plasma parameters achieved in tokamaks. There are several areas where the understanding of processes and measurement of parameters in the SOL can lead to improvements of the central plasma. One topic of SOL plasma research has been the determination by which process [1] (sputtering, evaporation, arcing etc.) and under what conditions (ohmic, auxiliary heating), impurities are generated at material surfaces surrounding the plasma. A companion topic is the study of methods that can be used to reduce the impurity flux entering the main plasma (poloidal and bundle divertors, ergodic limiters).

The second area of interest in the SOL plasma stems from the inferences that can be drawn about transport processes occurring within $r = a$. For example, poloidal asymmetries in electron density and density e-folding length ($\lambda_n$) have been detected for $r \geq a$ in plasmas with poloidally symmetric limiters [2]. Particle and/or heat transport, for $r \leq a$, must also be poloidally asymmetric. The total heat flux into the SOL plasma has also been found to be poloidally asymmetric in diverted plasmas through measurements of the divertor plate heat loads [3,4].

A third reason for interest in the SOL plasma derives from the effect of edge plasma conditions on central plasma confinement in the case of poloidally-diverted, neutal-beam heated "H-mode" discharges [5–7]. If the level of neutral pressure in the SOL is too high, "H-mode" is not achieved. In fact, there is direct evidence of an inverse linear dependence between the edge neutral pressure and $\tau_E$ [7], the global energy confinement time. Both low-$Z$ impurities and neutrals can cool the plasma just inside the separatrix.

The study of MARFE phenomena may have implications in all three areas of interest discussed above. MARFEs [8–16] are an axisymmetric, strongly radiating belt of short poloidal and radial extent located at the high-field edge of the plasma. The radial extent includes the SOL and extends to regions inside the divertor separatrix or limiter radius. The MARFE occurrence has been characterized by increases in local $n_e$, rms density fluctuation amplitude ($\tilde{n}^2$), edge density e-folding length ($\lambda_n$) in the SOL [11], and low-$Z$, low ionization state radiation in both the SOL and $r < a$ [8,10,11,13,17–19]. The electron temperature in this region decreases [11]. There is general agreement that the MARFE characteristics described above are explained by the occurrence of a radiation-driven thermal instability. However, in all tokamaks, the threshold in $\bar{n}_e$ for a MARFE occurrence scales linearly with plasma current. There has not been an explanation for the processes underlying such a dependence. In addition, in some cases the MARFE is a precursor to a density limit disruption [10,12].

Quite recently, a MARFE-like phenomenon, referred to as a "detached" plasma (DP), has been reported in the literature [13,20–23]. The DP is again characterized by large amounts of radiation from its boundary layer, but that boundary layer is at a radius less than that of the limiter. This radiation however, differs in character from the MARFE in that it is poloidally symmetric. In order for the plasma to be effectively detached from the limiter, the total amount of radiation must be approximately equal to the input power. Once the DP is formed, the minor radius as defined by the radius of the radiating boundary layer, can be varied by careful control of the plasma current, input power and $\bar{n}_e$ (fueling rate).

There are several important implications of the

* Work supported by US DOE Contract#DE-AC02-78ET51013.

MARFE phenomena described above. The strongly radiating regions at the edge of the plasma can account for a substantial fraction, if not all, of the input power, thus reducing heat fluxes to and impurity sources from the limiter/divertor surface due to evaporation and sputtering. In the case of the DP, contact with the limiter surface, and thus the impurity source, is further reduced by the reduction in $a$, the minor radius. Also, the radial extent of the MARFE overlaps the limiter or separatrix radius, indicating poloidal asymmetries occur on closed flux surfaces. A review of published data on MARFEs in tokamaks during strictly ohmic operation, shows that the MARFE occurs at values of $\rho$ in the range $0.4 \leq \rho \leq 0.7$ where

$$\rho = \frac{\bar{n}_e(10^{20}\ \mathrm{m}^{-3})}{I_p(\mathrm{MA})/\pi a^2(\mathrm{m}^2)}. \quad (1)$$

The density limit on these same tokamaks which can also be characterized by $\rho$, varies from $\rho = 0.5$ to $\rho = 1.0$. The $\rho$ threshold for the DP to occur is quite close (within 90%) to the density limit. Thus, even though the magnitude of edge parameters, and thus radiation, varies widely among tokamaks, trends in edge conditions which bring about MARFE phenomena (and most likely density limit disruptions) do not. This is confirmed by a review of edge plasma measurements from a number of tokamak experiments.

## 2. Review of experimental data

### 2.1. Characteristics of MARFEs

MARFEs are a common occurrence on most tokamaks [8–17]. The major characteristics of a MARFE, such as its radiative nature and location at the high-field edge of the plasma, are quite consistent among those experiments. This paper will explore these commonalities as well as make some effort to explore the differences.

The occurrence of a MARFE is most often determined by some combination of radiation-measuring diagnostics. An example from Alcator-C [11], is displayed in fig. 1 where the MARFE begins at 120 ms. Two vertical chords of the density interferometer ($\lambda = 119\ \mu$m) are displayed: at the onset of a MARFE, the signal is lost on the chord which passes through the MARFE region (a) while the chord that passes through the plasma center (b) is unaffected (other than a slight amount of noise which is not discernible in this figure). A bolometer detector (c) measuring total radiated power along essentially the same vertical chord as trace (a) indicates large increases in emission from the MARFE region. Similar effects are found with such line emissions as $H_\alpha$ (d) and CIII (e). Line emission from higher ionization states of carbon and other low-$Z$ impurities in Alcator-C are not as strongly affected.

The radiated power from the MARFE region is

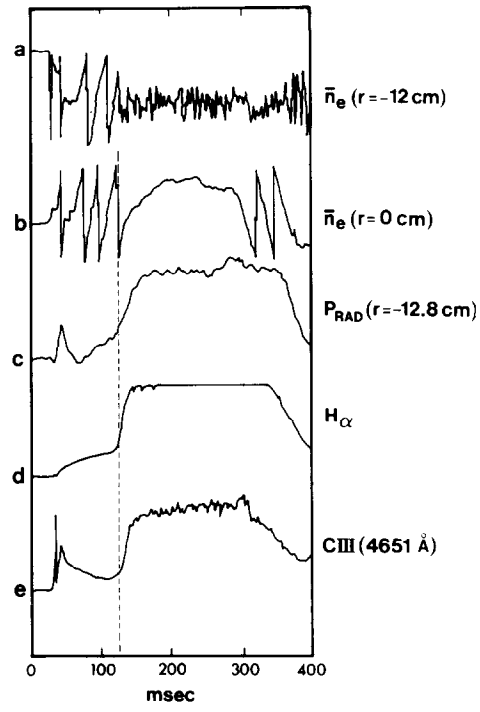


Fig. 1. Diagnostic traces versus time: The MARFE occurs at 120 ms and continues for the remainder of the discharge; (a) inside (−12 cm) vertical density-interferometer chord; (b) central density-interferometer chord; (c) inside (−12.8 cm) vertical bolometer chord; (d) $H_\alpha$ emission (horizontal view) which saturates after MARFE onset; (e) CIII line emission (vertical view, 4651 Å).

dominated by line emissions from these low-$Z$ impurities [11,13]. In particular, oxygen and carbon are found to account for the large local emission rates determined from bolometric measurements [11]. Fig. 2 shows an example, during a MARFE, from the JET tokamak of the relative enhancement of a number of impurity line emission magnitudes during a MARFE [13]. The magnitudes of local emissivities in the MARFE region have been inferred to be similar to the ohmic input power at the plasma center [11,17] (e.g. 10 W/cm$^3$ on Alcator-C).

Most aspects of the size and location of the MARFE are also consistent among different tokamaks. The MARFE is localized about a particular poloidal angle and appears to start simultaneously at all points toroidally. The radial extent is limited to about 10% of the plasma minor radius on the midplane. This radial extent straddles $r = a$. Effects are noted in the edge plasma by Langmuir probes [11].

The changes which are found in the emission from higher ionization states of low-$Z$ impurities are somewhat ambiguous in inferring MARFE effects at radial locations within $r = a$. The loss of signal from the density-interferometer chord signal pictured in fig. 1(a) is less ambiguous evidence of MARFE effects within

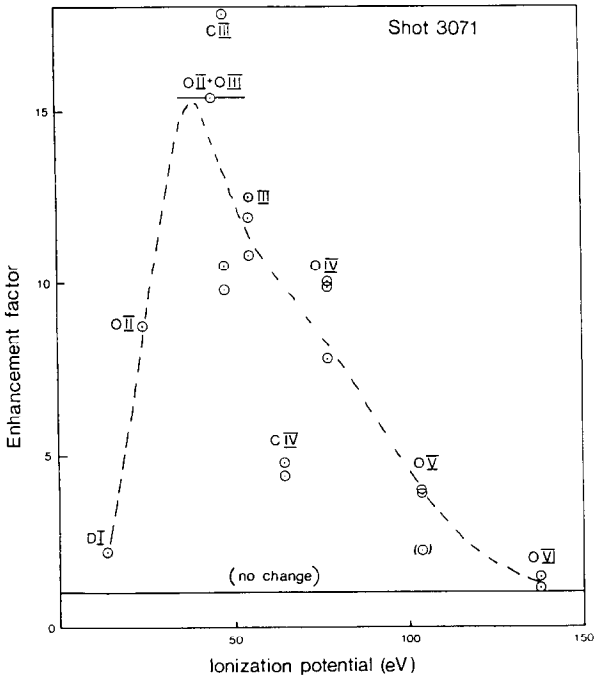


Fig. 2. Enhancement of line brightness during a MARFE in the JET tokamak.

the main plasma. These diagnostic chords pass between two full poloidal ring limiters which are separated toroidally by 4 cm. The effect of the SOL plasma on these signals is negligible. Therefore, when the MARFE occurs, the signal is lost due to effects within $r = a$.

An illustration of the MARFE location in poloidal angle ($\theta$) is provided by fig. 3 where $\theta$ is zero at the outside midplane. The poloidal extent is typically 30° being confined to the high-field edge of the plasma ($90° \leq \theta \leq 270°$ in fig. 3). Within that region, the MARFE has been found in the following variety of locations: ASDEX [10], FT [12] and D-III [9] generally find the MARFE to occur on the mdiplane ($\theta = 180°$); Alcator-C [11], JET [13] and TFTR [17] find the location to be above the midplane ($\theta \approx 235°$). It should be noted that the location of the MARFE in the latter two tokamaks is the final location. As the density is increased, the MARFE, in these two large tokamaks, first appears at a point symmetric about the midplane ($\theta \approx 125°$) and then moves, over a long period ($\simeq 100$ ms) to the final location in the upper half of the machine [11]. In TFTR [17], the symmetry of this process can be reversed with the reversal of the toroidal magnetic field direction. For the location of the MARFE above the midplane in JET, TFTR, and Alcator-C, the direction of the magnetic field is such that $\boldsymbol{B} \times \nabla \boldsymbol{B}$ is up. The poloidal location can also be modified by vertically displacing the plasma from a centered position [10] or by application of neutral beam heating [10,17].

There have been several direct measurements of

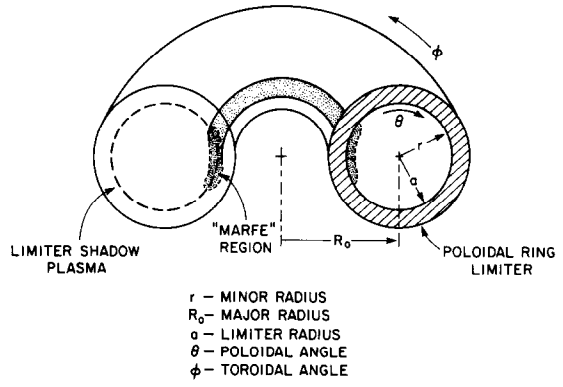


Fig. 3. Illustration of the toroidal nature of the MARFE. The poloidal angle, $\theta$, is measured from the outside midplane. The poloidal ring limiter radial extent is indicated by the cross-hatched area.

plasma parameters within the MARFE region in Alcator-C [11]. These include Langmuir probes and crossed-beam correlation techniques from $CO_2$ laser-scattering. The $CO_2$ scattering measurments show that prior to a MARFE occurence, density fluctuations are largest at the location where the MARFE will occur. Furthermore, after onset of a MARFE, the fluctuation amplitude ($\tilde{n}^2$) increases by at least two orders of magnitude and spreads across the top edge of the plasma with the peak in $\tilde{n}^2$ still at the MARFE location. The density in the MARFE region ($r \geq a$) was measured by insertion there of a Langmuir probe. A density increase is typically observed during the MARFE to be of order $0.5–1.0 \times n_{e0}$, the density at the plasma center. The density e-folding length ($\lambda_n$) roughly doubled during the MARFE. But of greater importance, it was found that the local electron temperature dropped significantly (to half its original value).

Futher estimates of the electron density in the MARFE region have been made through examination of signal changes on density-interferometer chords which pass through the MARFE region by deducing the chordal pathlength through the MARFE from other diagnostics [9,10,13,17] (e.g. visible camera pictures). On other than high-magnetic field tokamaks, this calculation again yields average densities in the MARFE region in the range $0.5–1.0\ n_{e0}$. As stated earlier, the density-interferometer chord which passes through the MARFE region in Alcator-C is lost during a MARFE occurence. This is not due to beam absorption ($n_{e,\mathrm{cutoff}} = 7.9 \times 10^{16}\ \mathrm{cm}^{-3}$) but is most probably caused by refraction of the beam due to large density gradients perpendicular to the beam.

### 2.2. Scaling

The central plasma conditions under which MARFEs will occur can be predicted to a large extent. The principal parameters with which the onset of MARFEs

have most often been correlated are: plasma current ($I_p$), line-averaged density ($\bar{n}_e$), and discharge cleanliness. In general, the MARFE is reported to occur for $\bar{n}_e$ greater than some threshold density, $n_m$, which increases linearly with plasma current [9,11]. A plot of such data from Alcator-C, where the MARFE occured during the constant current phase of the discharge, is shown in fig. 4. The plasma current is normalized by the poloidal crossectional area, $\pi a^2$ which allows Alcator-C discharges of various minor radii to appear on the same plot. Data are displayed from plasmas with the standard Alcator-C geometry of $R = 64$ cm, $a = 16.5$ cm with deuterium (▼) and helium (◇) fill gases. For 10 cm minor radii plasmas, MARFEs were observed for $R =$ 57.7 (□) and 70.5 (○) cm. The solid line, which is a fit to the above data, corresponds to a value of $\rho = 0.55 \pm 0.05$. MARFEs in pellet-injection fueled plasmas (△) occur at a significantly higher value of $\rho = 0.75 \pm 0.05$ ($R = 64$, $a = 16.5$, D → H). The density limit for gas-fueled discharges on Alcator-C corresponding to the lower boundary in a Hugill plot is represented on this plot by the line $\rho = 1$.

MARFEs were absent from the flattop (constant plasma current) portion of smaller radii ($a = 10$, 13 cm), but centered ($R = 64$ cm) Alcator C plasmas. Occasionally, when $\rho > 0.8$ during current rampdown, MARFEs did occur. The absence of MARFEs in small minor radius plasmas has also been reported to occur in TFTR [17]. It is possible that wall proximity somehow affects the neutral or impurity density at the plasma edge. There have been no experimental measurements to indicate whether this is true or not.

The above scaling can be applied to all available tokamak data on MARFEs. Table 1 is a summary of

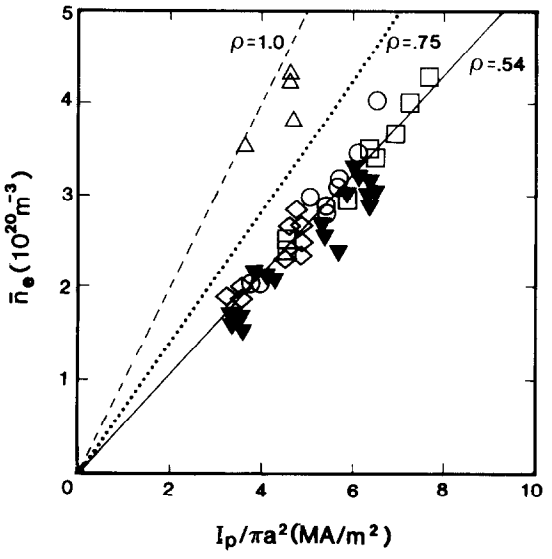


Fig. 4. For Alcator-C plasmas, the line-averaged density, $\bar{n}_e$, at which a MARFE starts is plotted versus $\kappa J$, the normalized current density. Several cases are included: ▼, $R = 0.64$, $a =$ 0.165 m, $D_2$ gas; ◇, $R = 0.64$, $a = 0.165$ m, He gas; □, $R = 0.577$, $a = 0.10$ m, $D_2$ gas; ○, $R = 0.705$, $a = 0.10$ m, $D_2$ gas; △, $R = 0.64$, $a = 0.165$ m, $D_2$ pellet into $H_2$ discharge.

this data with $\rho$ (eq. (1)) used to parameterize the MARFE threshold. Clearly such a tabulation of data is subject to variations among the different tokamaks in the criteria used for determining the occurence of a MARFE. In addition, published papers do not present a large database from each machine. Even so, some general trends can be seen: the $\rho$ factor accounts for the

Table 1

| Machine | $R$(m) | $a$(m) | $B_t$ (T) | $\kappa$ | $Z_{bg}$ | $\rho = \frac{\pi a^2 \bar{n}_e}{I_p}\left(\frac{10^{20}}{\text{MA m}}\right)$ | | Comments [a] |
|---|---|---|---|---|---|---|---|---|
| | | | | | | MARFE | Disruption | |
| ALCATOR C | 0.64 | 0.165 | 6–10 | 1 | 1 | 0.5 ±0.05 | 1 | 1 |
| | 0.577 | 0.1 | 8 | 1 | 1 | 0.5 ±0.05 | | 1 |
| | 0.705 | 0.1 | 8 | 1 | 1 | 0.5 ±0.05 | | 1 |
| | 0.64 | 0.165 | 8 | 1 | 2 | 0.5 ±0.05 | | 1 |
| | 0.64 | 0.165 | 8 | 1 | 1 | 0.75±0.05 | 1 | 1,2 |
| ASDEX [10] | 1.65 | 0.4 | 2.2 | 1 | 1 | 0.7 ±0.05 | 1 | 1,3 |
| | 1.65 | 0.4 | 2.2 | 1 | 1 | 0.85±0.05 | 1.5 | 1,3,4 |
| D-III [9] | 1.4 | 0.4 | 2 | 1 | 1 | 0.45 | 0.75 | 1 |
| | 1.4 | 0.4 | 2 | 1.4 | 1 | 0.32 | | 1 |
| DITE [23] | 1.17 | 0.26 | 2.7 | 1 | 1 | 0.55 | 0.6 | 1 |
| | 1.17 | 0.26 | 2.7 | 1 | 2 | 0.55 | 1 | 1 |
| FT [12] | 0.83 | 0.2 | 6–8 | 1 | 1 | 0.75±0.05 | 1 | 5 |
| JET [13] | 2.96 | 1.25 | 2.5–3.4 | 1.2–1.6 | 1 | 0.55–0.3 | 0.7–0.5 | 1,5 |
| TFTR [17] | 2.5 | 0.82 | 4 | 1 | 1 | 0.4 ±0.05 | 0.7 | 1 |
| | 2.5 | 0.82 | 4 | 1 | 2 | 0.8 ±0.05 | 1.0 | 1 |

[a] Comments: 1–constant plasma current. 2–pellets. 3–diverted. 4–neutral beam injection. 5–falling plasma current.

MARFE threshold reasonably well over a wide range in current (0.1–1.8 MA), toroidal magnetic field (2–10 T), and $\bar{n}_e$ ($0.1–4.0 \times 10^{14}$ cm$^{-3}$). In ref. [9] it was suggested, and the data from D-III [9] and JET [13] imply that a $\kappa$ (elongation) dependence should be added. The remaining variation of $\rho_m$ evident in this tabulation could possibly be accounted for by $Z_{eff}$ or discharge cleanliness variations. On tokamaks other than Alcator-C and DITE (with He fill gas), the MARFE occurs close to the density limit ($\rho_m \approx 0.8\rho_{dis}$). This includes cases where the disruption limit is low (D-III, DITE, JET, TFTR) and where $\rho_{dis} = 1$ (ASDEX, FT; falling plasma current).

A number of variations can be seen in this table which may be clues to understanding MARFEs. In DITE [23] and Alcator-C the use of helium as a fill gas does not affect the MARFE threshold. This differs from TFTR [17] where the MARFE threshold increases by a factor of 2 in changing the fill gas to helium. The two largest values of $\rho_m$ are from ASDEX and FT tokamak data. ASDEX is the only diverted tokamak included in this table; some or all of the FT data are from the falling current portion of the discharge.

### 2.3. MARFEs and the disruption limit

The disruption limit is often correlated with the MARFE threshold. For example, in ASDEX [10] and FT [12] plasmas, as the density is raised above the MARFE threshold, MHD behavior (increased $m = 2$ fluctuation amplitude) starts, the temperature profile shrinks and a disruption ensues. This behavior has not been as thoroughly documented on the other tokamaks but the MARFE threshold, as discussed earlier, does occur close to the density limit in H or D fill gas discharges. In addition, when ASDEX plasmas are heated with neutral beams, the MARFE threshold and density limit are both increased.

### 2.4. Detached plasmas (DP)

Recent studies of MARFEs and disruptions have revealed a new poloidally symmetric radiation phenomenon called a detached plasma (DP) [13,20,21]. The data base concerning the subject of the DP is not as extensive as for MARFEs but it is the subject of ongoing research [22,23]. Several general characteristics can be described: a region of strong radiation emissivity at the plasma boundary is formed which is approximately uniform in poloidal and toroidal angles with the total amount of radiation roughly equal to the input power. The heat flow to the limiter in these cases decreases to approximately zero ($P_{lim} \ll P_{in}$), with the plasma minor radius (the radius of the radiative layer) smaller than the limiter radius, thus the derivation of the name detached plasma. Similar to MARFEs, the radiation is attributed to low-$Z$ impurities [23].

Detached plasmas are obtained by increasing $\rho$ past MARFE threshold, $\rho_m$, towards the density disruption limit. This has the effect of increasing the radiated power ($P_{rad}$) to $\approx 100\%$ of the input power ($P_{in}$) at which point the plasma either disrupts or detaches. The safest way to cause a detached plasma, rather than a disruption, is to reduce the plasma current while holding $\bar{n}_e$ approximately constant [13,20]. The DP has also been achieved by the alternative method; increasing $\bar{n}_e$ while holding $I_p$ constant [22,23]. With either method of obtaining a DP, the threshold for its occurence, $\rho_{dp}$, is close to the density disruption limit, $\rho_{dis}$. The closeness of the two thresholds is due to the criterion $P_{rad} \approx P_{in}$ which holds true in both situations. This very close correlation of $\rho_{dp}$ and $\rho_{dis}$ is further demonstrated in DITE [23], where both the DP and disruption thresholds are increased by a factor of 2 in the changeover of fill gas from hydrogen (or deuterium) to helium. The exact timing with respect to detachment (100% radiation) by which the poloidal radiation emission profile changes from poloidally peaked (MARFE) to uniform has not been clarified at this time.

A typical case of a DP created by a reduction in plasma current is shown in figs. 5 and 6, reprinted from ref. [20]. As the plasma current is reduced, the magnitude of the in–out asymmetry in radiation brightness evident in fig. 5 (the MARFE), increases. The transition period (shaded region) is characterized by surface loop voltage increase (fig 6a; 1.9 s) and a reduction in $\bar{n}_e$ (fig. 6(b)) and central temperatures (fig 6(c)). Also during this transition period, the peak in radiation emission, which was the MARFE, increases in magnitude and spreads poloidally around the machnie (shaded

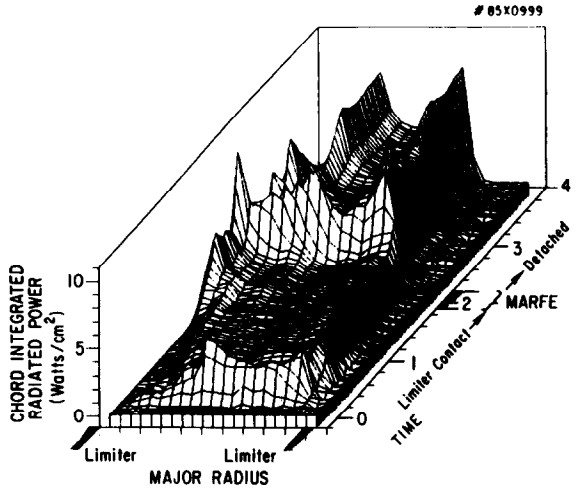


Fig. 5. Radiation brightness versus time measured by a vertically viewing bolometer array in TFTR during a discharge further illustrated in fig. 6. The in–out asymmetry in brightness which appears at $\approx 1.3$ s is the MARFE. The shaded region indicates a transition to DP starting at about 1.9 s.

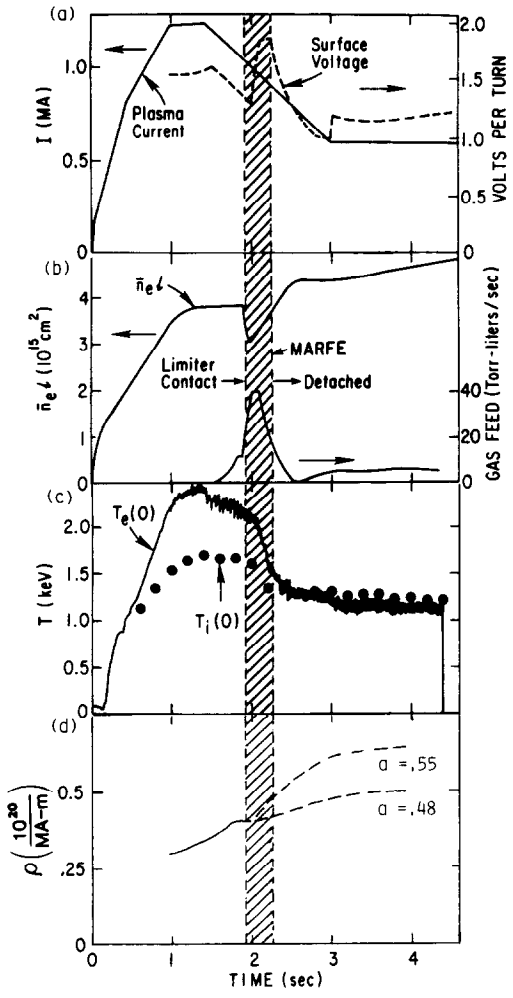


Fig. 6. Diagnostic traces versus time for the TFTR discharge shown in fig. 5: (a) Plasma current and surface loop voltage; (b) $\int \bar{n}_e dl$ and gas feed rate; (c) central electron and ion temperatures; (d) $\rho = \bar{n}_e/(I_p/\pi a^2)$ for two different estimated final radii.

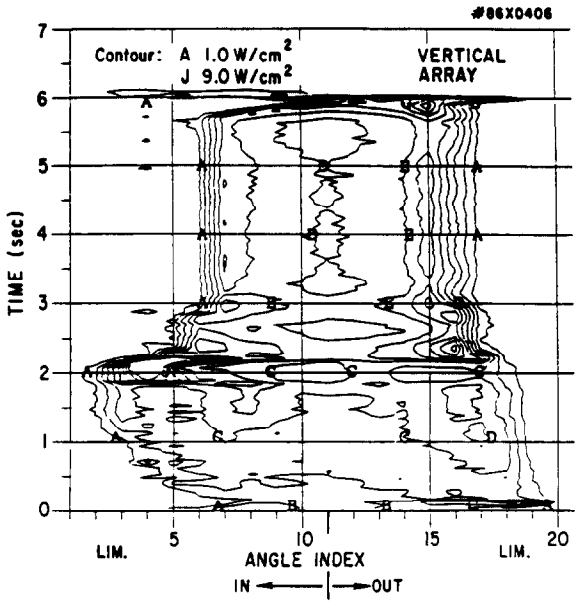


Fig. 7. Contour plot of the bolometer brightness shown in fig. 5.

period – fig. 5). At the end of the transition period the plasma minor radius has shrunk away from the limiter and the radiated power has become poloidally symmetric. The bolometer brightness data from fig. 5 are replotted in a contour format in fig. 7. It is evident that the minor radius of the plasma continues to shrink as the plasma current is reduced until $t = 3$ s. The final minor radius has been estimated for this discharge to be $a = 0.55$ m [20]. Fig. 6(d) includes a calculation of $\rho$ versus time for this discharge under the assumption that the final minor radius is either 0.55 m as described above as well as for $a = 0.48$ cm. This latter estimate is obtained from measuring the distance between radiation emission peaks from fig. 3(b) of ref. [20]. Utilizing the radiation emissivity peaks to determine the minor radius, a survey of $\rho$ in a number of TFTR DP discharges has been carried out [22] which indicates that, in general, $\rho \lesssim 0.5$.

Once the plasma is detached, the minor radius can be estimated from the radial position of peaks in line emission, as well as bolometer, Thomson scattering and density-interferometer measurements. There is, as yet, no uniform method for determining the minor radius, however, the plasma edge conditions adjust to continue radiating away the input power. This can be understood by examining the amount of power radiated by a thin layer of fixed thickness, $w$, at the plasma edge;

$$P_{rad} \approx P_{in} \propto awn_{eb} n_{zb} L_z(T_{eb}), \tag{2}$$

where the subscript b signifies a boundary layer parameter. As will be discussed later, $n_{eb} \propto (\bar{n}_e/I_p)^\gamma$ in *attached* plasmas. For lack of better data, this dependence will be used for the DP as well. In addition, experiments on TFTR [24] and JET [25] have found $Z_{eff} \propto 1/(\bar{n}_e/I_p)^\gamma$. This will be interpreted here to imply that $n_{zb} \approx$ constant, independent of $\bar{n}_e/I_p$. This is a conservative estimate of $n_{zb}$ because as $\bar{n}_e$ is increased the plasma becomes more opaque to entering neutral impurities implying a larger ratio of $n_{zb}/n_{z,plasma}$. Eq. (2) can then be rewritten

$$P_{rad} \propto \left(\frac{\bar{n}_e}{I_p}\right)^\gamma aL_z(T_{eb}). \tag{3}$$

The strong inverse dependence of the carbon cooling rate on $T_{eb}$ for temperatures of interest (7 eV $\leq T_{eb} \leq$ 30 eV) effectively increases the value of $\gamma$ in eq. (3) due to the roughly inverse dependence of $T_{eb}$ on $n_{eb}$. But for the purpose of this discussion this dependence will not explicitly be included. Therefore, if $P_{in}$ and thus $P_{rad}$

are held constant as $\bar{n}_e$ is increased, the minor radius, $a$, would tend to decrease. Similarly, if $\bar{n}_e$ were held constant but $P_{in}$ increased, $a$ would tend to increase. This rough correspondence between $P_{rad}$, $a$, and $\bar{n}_e$ is seen in TFTR experiments [22].

The central plasma parameters of the DP are similar to those of standard attached discharges: energy confinement time [20] is predicted by neo-Alcator scaling [26], sawteeth occur on soft X-ray emission, $n_e$ and $T_e$ profile shapes are standard. DITE [23] reports similar concentrations of low-$Z$ impurities. TFTR [22] and DITE [23] find fewer high-$Z$ impurities in the DP. The similarity of low - $Z$ concentrations in both attached and detached plasmas is incongruous since the direct interaction of the plasma with the limiter (made of graphite) has supposedly been eliminated. This area certainly deserves further study. One significant change found in the absence of limiter contact is that fueling of the plasma by gas puffing becomes more efficient [13].

## 3. MARFE theory

As discussed earlier, the MARFE is generally considered to be the result of a radiation thermal instability. In examining a particular region at the plasma edge to determine if it is thermally stable, a necessary condition for a MARFE to occur is that the local temperature be above that where the radiation cooling rate, $L_z(T_{eb})$, is a maximum (i.e. $dL_z/dT < 0$). Then, a local temperature decrease in that region causes two principal effects: both the heat conduction along a field line to that region and the radiation loss will increase. If the radiation increase is larger than the conduction increase, the local volume is thermally unstable; the radiation increase causes the local temperature to decrease further, etc. It is only at the plasma edge where parallel conductivity is low that a local effect can be found.

### *3.1. Stability*

Some simple efforts were made in initial reports to model the stability of this situation [9,11]. Recently more thorough modelling [15,16] has been performed and will be reviewed here. The particle, momentum, and energy equations are used as a starting point:

$$\frac{\partial n}{\partial t} + \frac{\partial (n v_\parallel)}{\partial s} = 0, \tag{4}$$

$$nm\frac{\partial v_\parallel}{\partial t} + nmv_\parallel \frac{\partial v_\parallel}{\partial s} + \frac{\partial (2nT)}{\partial s} = 0, \tag{5}$$

$$3\frac{\partial (nT)}{\partial t} = \frac{\partial}{\partial s}\left( K_\parallel \frac{\partial T}{\partial s} - 5nTv_\parallel \right) + \frac{1}{r}\frac{\partial}{\partial r}\left( rK_\perp \frac{\partial T}{\partial r} \right) - \sum nn_z L_z(T), \tag{6}$$

where $n = n_{eb} = n_{ib}$, $n_{zb}$ is the impurity density, $s$ denotes distance along a field line, $K_\perp$, $K_\parallel$ are perpendicular and parallel conductivities (ions and electrons) respectively. Defining $\Theta = B_{pol}/B_{tor} = r/Rq$, for cylindrical $q$, the derivatives along field lines can be converted to derivatives in poloidal angle

$$\frac{\partial}{\partial s} = \frac{\Theta}{r}\frac{\partial}{\partial \theta}. \tag{7}$$

An analytic stability condition can be derived from the above equations [15,16] for the case of an initial equilibrium with pressure remaining constant on a flux surface ($n = n_0$, $T = T_0$, $\partial n/\partial\theta = \partial T/\partial\theta = 0$) and no plasma flows. Then the above equations can be linearized, using a temperature perturbation of the form:

$$T = T_0 + T_1; \tag{8}$$

$$T_1 = \tilde{T} e^{\gamma t} \cos m\theta. \tag{9}$$

A symmetric form for the density follows from eq. (9) and the condition of pressure constancy on a flux surface. Futher simplifying assumptions can be made: $n_{z0} = \alpha n_0$, $\tilde{n}_z = \alpha\tilde{n}$ and

$$\frac{1}{r}\frac{\partial}{\partial r}\left( rK_\perp \frac{\partial T}{\partial r} \right) = \frac{-K_\perp}{\Delta^2}\tilde{T}, \tag{10}$$

where $\Delta$ is the radial half width of the perturbed layer. A dispersion relation is obtained [15,16] from which the following condition for instability ($\gamma > 0$) is derived:

$$K_\parallel k_\parallel^2 + \frac{K_\perp}{\Delta^2} + \alpha n_o^2 \frac{dL_z}{dT} - \frac{2\alpha n_0^2 L_z}{T} < 0, \tag{11}$$

where

$$k_\parallel^2 = m^2\Theta^2/r^2.$$

As stated earlier, the occurrence of the MARFE is due to the dominance of radiative terms (last two) over heat conduction (first two terms). In ref. [15], this stability criterion is evaluated using Alcator C conditions with reasonable success. A modified form of the coronal $L_z$ for carbon is used to take into account non-coronal equilibrium. The perpendicular heat conduction term (second from left in eq. (11)) is found to be small in relation to parallel conduction. A more accurate application of this criterion would involve the use of more realistic numerically calculated non-coronal models for $L_z$ [27].

### *3.2. Poloidal equilibrium*

The previous discussion outlined under what conditions a thermal instability would start growing, but not its subsequent evolution and final state. Through time-dependent numerical modelling of hydrogenic and impurity ion fluids along a field line after a perturbation was introduced, Neuhauser [16] was able to provide information in both these areas. The basic characteristics of the MARFE are evident in the results of this model: density higher, temperature lower in the MARFE region (at the final state) with radiation due mainly to

low-ionization states of impurities. The impurity density is peaked away from the MARFE region where the radiation emission is highest. This behavior may explain the dependence of C-III radiation before and during a MARFE found in ref. [11].

An analytic prediction of possible poloidal boundary temperature ($T_{eb}$) equilibria is given by Stringer [15]. With analytic fits to the coronal $L_z$ cooling rate for carbon, and the assumption of poloidally symmetric perpendicular heat flow ($Q_\perp$) from the main plasma, solutions to the energy conservation equation, eq. (6), were found. Since impurity radiation is the only loss mechanism included in eq. (6), (i.e. no losses to limiter or divertor plate) equilibria could be found only for high edge densities (high radiation loss). Significantly, solutions with both poloidally symmetric (DP-like) and asymmetric (MARFE-like) temperature profiles were found by this method.

There are several constraints in Stringer's model, which if modified, might change the results significantly. In particular, no losses, other than radiation were included. The radiated power is forced to be equal to the input power. This is realistic for the DP but not neccesarily for the MARFE. Perhaps more relevant to a discussion of poloidal profiles is the assumption of poloidally uniform perpendicular heat flux. This assumption has been found not to be true in divertor tokamaks. In addition, a poloidally varying $Q_\perp$ is used to explain the location of the MARFE at the high-field edge of the plasma [11,15]. The use of an analytic fit of carbon coronal equilibrium cooling rates should not significantly affect the existence of the types of equilibria found.

## 4. Discussion

MARFEs and the related phenomenon, detached plasmas (DP), are both clear evidence of thermal instabilities occurring at the edge of tokamak plasmas. A number of questions are raised by the phenomenology of MARFEs and DPs which may have wider implications for understanding tokamak physics.

### *4.1. Relationship of MARFE to boundary and central parameters*

Clearly, even though these MARFE phenomena are manifestations of a thermal instability driven by atomic physics, its occurrence can be predicted with reasonable accuracy under a wide variety of tokamak conditions. The process or trend that occurs to precipitate a MARFE or DP must be a strong function of $\bar{n}_e/I_p$ so that these variations in discharge conditions between experiments have little effect.

One possible candidate for this process is the nonlinear dependence of the boundary layer density, $n_{eb}$, on $\bar{n}_e$ or $(\bar{n}_e/I_p)$ that is detected either directly by Langmuir probe measurements [28–31] or indirectly by measurment of $H_\alpha$ emission [32] on a number of tokamaks. An example of such data from Alcator-C [28], taken with Densepack [33], a poloidal array of Langmuir probes located in the SOL plasma, is shown in fig. 8. These data represent a poloidal average of densities measured at a minor radius of 16.8 cm ($a = 16.5$ cm) by 10 probes spread in poloidal angle at one toroidal location. The data are plotted versus $\rho$, as defined in eq. (1). These discharges are characterized by a toroidal magnetic field of 6 T with hydrogen fill gas. Note the change in slope and scatter in data for $\rho > \rho_m \approx 0.55$. Above the MARFE threshold, $\rho$ is clearly no longer the proper plotting parameter. Data taken during discharges where no MARFE was evident are indicated by closed circles. Also presented are $n_{eb}$ data taken during discharges where the MARFE was found to occur either during the short data sampling period (open squares) or at another time during the experiment (open circles). A multiple parameter, nonlinear regression fit to a similiar set of data [28], for $\rho < 0.5$, yields a power law dependence of $n_{eb} \propto \rho^\gamma$, $\gamma = 4.0 \pm 1$.

A logical connection based on energy considerations can be made between these edge parameter data and the MARFE threshold. The power radiated by the boundary plasma is described in eq. (3). Given the $\rho$ dependence of $n_{eb}$ exhibited by the data of fig. 8, $P_{rad}$(from the SOL) would increase much faster than $P_{in}$, which weakly depends on $\rho$. As the fraction of input power radiated by the edge plasma increases, the edge temperature

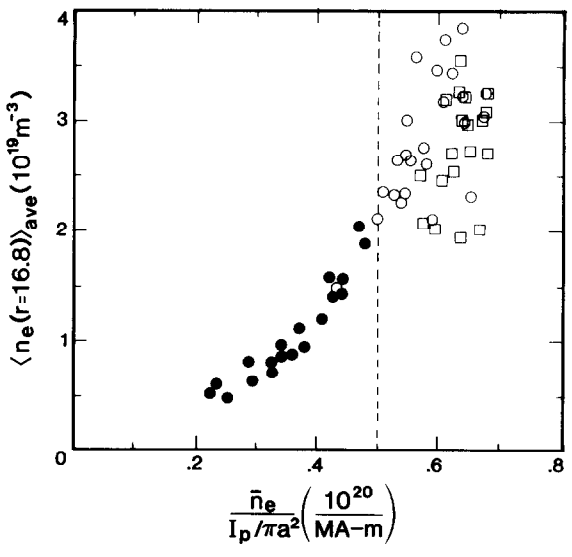


Fig. 8. Poloidally averaged boundary layer density, $n_{eb}(r = 16.8)$, measured by Densepack Langmuir probe array in Alcator-C. The limiter radius was 16.5 cm, $B_{toroidal} = 6$ T, $D_2$ fill gass: ●, no MARFE during discharge; other cases are with MARFE occurrence either during (□) or not during (○) the sampling period for this data. MARFE threshold is $\rho_m = 0.55 \pm 0.05$.

decreases. Examining the MARFE stability condition, eq. (11), this reduction in $T_{eb}$ has the effect of decreasing the stabilizing conduction term ($\propto T_{eb}^{5/2}$), while increasing the radiative (destabilizing) terms, $2L_z/T_{eb} - dL_z/dt(\propto T_{eb}^{1.5}$; for $T_{eb} < 7$ eV and coronal cooling rates for carbon). The destabilizing terms also increase proportional to $n_{eb}^2$ ($\propto \rho^6$). Therefore, as $T_{eb}$ decreases, eq. (11) is more likely to be satisfied (MARFE). This nonlinear dependence of $P_{rad}/P_{in}$ on $\rho$ has been observed in JET [34].

This reasoning can be carried further. Due to the nonlinear dependence of $P_{rad}$ on $\rho$, but essentially linear dependence on $n_{eb}$, an increase in impurity density would translate into a smaller fractional decrease in $\rho_m$. But certainly it is still true that $\rho_m$ can be significantly affected by machine cleanliness.

Auxiliary heating and pellet injection have been shown to significantly increase the MARFE threshold, $\rho_m$ (see table 1). This can be explained, in the context of the above qualitative arguments, as an increase in $T_{eb}$ and decrease in $n_{eb}$ respectively, for a given value of $\rho_m$. In particular, such a change in SOL parameters for a given $\rho$ is seen in the comparison of the data of fig. 8 with a set of pellet-fueled discharges in Alcator-C (fig. 9). Pre-pellet $n_{eb}$, where no MARFE activity was evident are indicated in fig. 9 by solid circles. The post-pellet data for cases where the relative change in line-averaged density, $\delta\bar{n}_e/\bar{n}_e^{pre} \gtrsim 1$ (open squares), show a similar trend versus $\rho$ as the pre-pellet data but shifted to larger values of $\rho$. The triangle data are post-pellet $n_{eb}$

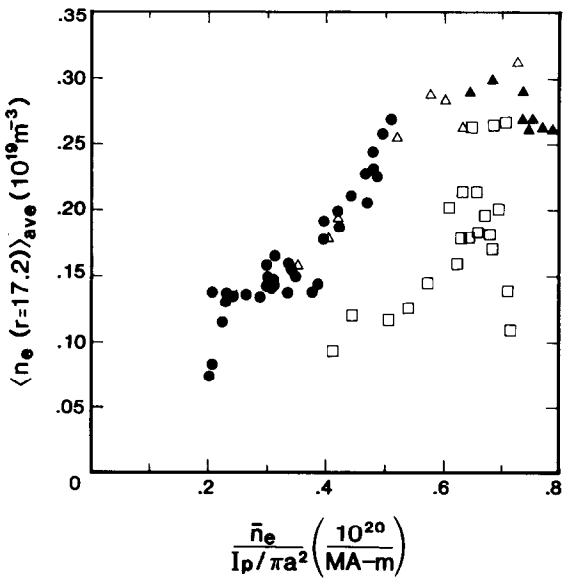


Fig. 9. Poloidally averaged boundary layer density, $n_{eb}(r = 17.2)$, measured by Densepack Langmuir probe array in Alcator-C for pellet fueled plasmas. Otherwise conditions same as fig. 8: ●, before pellet data, no MARFEs occured; △, after pellet, $\delta\bar{n}_e/\bar{n}_e^{pre} < 1$, no MARFE; ▲, after pellet, $\delta\bar{n}_e/\bar{n}_e^{pre} < 1$, MARFE; □, after pellet, $\delta\bar{n}_e/\bar{n}_e^{pre} > 1$, no MARFE.

where $\delta\bar{n}_e/\bar{n}_e^{pre} \lesssim 1$ and are divided into cases where the pellet either caused a MARFE (solid traingles) or not (open triangles). It is clear that the pellet allows larger values of $\rho$ to be accessed at a given value of $n_{eb}$, and thus, without a MARFE occurence.

The relatively low edge density at high $\rho$, *after* injection of a pellet with large $\delta\bar{n}_e/\bar{n}_e^{pre}$ is correlated with increases in $\rho_m$ as well as central particle confinement, $\tau_{p0}$ [35]. $\tau_{p0}$ has been found to degrade for $\rho \geqslant 0.75$.

Global particle confinement ($\tau_p$) is more relevant to a discussion of the SOL density. In several tokamaks, $\tau_p$, as determined by $H_\alpha$ measurements, decreases as $\bar{n}_e$ is increased [32,36,37]. In particular, data from TFTR [36] indicates that $\tau_p \propto (\bar{n}_e/I_p)^{-3}$ (i.e. $\rho^{-3}$). The relevance to Alcator-C $n_{eb}$ data can be seen from the relation

$$\frac{N}{\tau_p} \approx \int_s D_\perp \frac{\partial n}{\partial r}\, dS, \tag{12}$$

$N$ is the total number density in the plasma ($\propto \bar{n}_e$) and the intergral is performed over the plasma surface defined by the limiter radius. This can be evaluated, giving

$$\frac{\bar{n}_e}{\tau_p} \propto \frac{\langle D_\perp\rangle\langle n_{eb}\rangle}{\langle\lambda_n\rangle} \tag{13}$$

where geometrical factors have been dropped and $\langle\ \rangle$ indicates a poloidal average. If $\langle D_\perp\rangle$ and $\langle\lambda\rangle$ do not depend strongly upon $\rho$ as $n_{eb}$ does, then through eq. (13) the probe results ($n_{eb} \propto \rho^3$) indicates that $\tau_p \propto \rho^{-3}$ similiar to the dependence measured in TFTR.

A decrease in $\tau_p$ (increase in $n_{eb}$) with increasing $\bar{n}_e$ is not neccesarily indicative of changing particle transport in the plasma within the limiter radius. It can also be attributed to the increasing opacity of the plasma to neutrals entering from the SOL. However, to explain the dependence on plasma current it seems there is no alternative explanation to that of changing particle transport properties within the limiter boundary.

### *4.2. Applications of MARFE phenomena research*

There are a number of areas where the study of the MARFE and DP could provide new insight into tokamak physics. To understand the density disruption limit, it is important to determine for what reason the plasma either disrupts or detaches as $P_{rad}/P_{in}$ approaches 1. As this limit is approached, the power flow to the limiter, and thus to the plasma at $r \approx a$, is reduced towards zero. Two factors could affect the evolution of the discharge either towards detachment or disruption at this radiation limit ($P_{rad}/P_{in} \approx 1$): first, if the symmetrization of edge radiation, and thus the transition to DP is "slower" than the rate of increase of $P_{rad}/P_{in}$, the plasma could disrupt. Second, the relative location of the radiation with respect to the limiter radius could be

important (i.e. whether the $q = 2$ surface is affected or not).

The transition from MARFE to DP may also provide information about perpendicular transport. The location of the MARFE at the high-field edge of the plasma, as opposed to any poloidal angle, has been attributed to poloidal asymmetries in perpendicular heat transport ($Q_\perp$) [11,15]. In experiment, the asymmetric nature of the MARFE is lost when the radiation limit is reached and the plasma detaches. One implication is that $Q_\perp$, if it were poloidally asymmetric to begin with, becomes poloidally symmetric after detachment. A second interpretation could be that $Q_\perp$ is poloidally asymmetric at all times: in *attached* plasmas the boundary condition imposed by limiter or divertor plate does not allow communication between high and low-field edges of the plasma. The result is a MARFE. When the DP is created, these boundary conditions are removed and transport along field lines dominates, effectively overcoming the effects of a poloidally asymmetric $Q_\perp(\theta)$. The corollary of such a hypothesis is that the MARFE starts at $r > a$. A thorough investigation should be made of the poloidal variation in $P_{rad}$ in the DP to determine if any poloidal asymmetries remain.

It would be advantageous to achieve H-mode confinement [5–7] in auxiliary heated non-divertor plasmas such as JET or TFTR. Detached plasmas might be a vehicle for achieving this result. Several necessary conditions can be abstracted from the existing database of H-mode plasmas [5–7]: the neutral density at the plasma edge should be low; the principal source of recycling should be removed from the plasma edge; and that $T_e$ should be large just inside $r = a$, which seems to be achieved above some input power threshold. The second condition is directly achieved by creating the DP. The first may be achieved by a combination of pumping and taking advantage of the large $\tau_p$ of detached plasmas. Failing that, increasing the input power, $P_{in}$, through non-ohmic means may overcome the convective (charge-exchange) losses that high edge neutral densities incur. However, $\bar{n}_e$ must be increased (through pellet injection) as $P_{in}$ is increased to keep reattachment from occurring. Work is underway at TFTR [22] along this line of reasoning.

## 5. Summary

MARFE phenomena are a common feature of tokamak discharges; they strongly affect the SOL plasma. The occurence of a MARFE can be predicted with reasonable accuracy over a wide range of plasma conditions and experiments to depend on $\rho = \bar{n}_e/(I_p/\pi a^2)$. Detached plasmas, a poloidally symmetric version of a MARFE, are more closely tied to the ratio $P_{rad}/P_{in}$ which appears to depend strongly on $\rho$. In general, where $\rho_m$ is close to $\rho_{dis}$, the central plasma parameters are affected. In those cases, as the density limit is approached, the MARFE is often the precursor to either a disruption or a DP.

Several implications can be drawn from the ability to use $\rho_m$ to predict a MARFE occurrence: the conditions for a MARFE, although tied to atomic physics, are determined by other processes which depend strongly on $\bar{n}_e/I_p$. The most likely process which is discussed in this paper is the scaling of density in the boundary layer $n_{eb} \propto \rho^\gamma$, with $\gamma = 4 \pm 1$ for $\rho \lesssim \rho_m$. This scaling appears to hold true on a number of tokamaks. This nonlinear increase in the SOL density also appears to be linked to the main plasma particle confinement.

Through examination of the properties of MARFES and DPs, topics concerning improvement and/or furthering the understanding of tokamak operation are considered. The MARFE threshold, $\rho_m$, can be increased by pellet injection, by decreasing the impurity density, and possibly through heating of the SOL plasma. Given the similar increase of $\rho_m$ and $\rho_{dis}$ on ASDEX with neutral beam heating, these methods hold hope for increasing the density limit still further. In addition, the detached plasma may provide the ability to achieve H-mode confinement in a divertorless tokamak as well as perhaps providing new insight into understanding perpendicular transport.

It is a great pleasure to acknowledge the invaluable discussions held with J.D. Strachan, S.S. Medley, G.M. McCracken and T. Stringer about detached plasmas and MARFEs, as well as with B. LaBombard, M. Greenwald and E. Marmar about boundary layer physics and particle confinement.

## References

[1] G.M. McCracken and P.E. Stott, Nucl. Fusion 19 (1979) 889.
[2] B. LaBombard and B. Lipschultz, PFC/JA-85-43, accepted for publication in Nucl. Fusion.
[3] D.K. Owens et al., J. Nucl. Mater. 93 & 94 (1980) 213.
[4] The ASDEX team, Max-Planck-Institut fur Plasmaphysik, Garching, Rep# IPP III/73
[5] F. Wagner et al., Phys. Rev. Letters 49 (1982) 1408.
[6] N. Ohyabu et al., Nucl. Fusion 25 (1985) 49.
[7] R.J. Fonck et al., in: Heating in Toroidal Plasmas, Proc. 4th Symp. Int. School of Plasma Physics, Rome, 1984 (ENEA, Frascati, 1984) p. 37.
[8] J.L. Terry et al., Bull. Amer. Phys. Soc. 26 (1981) 886.
[9] D.R. Baker, R.T. Snider and N. Nagami, Nucl. Fusion 22 (1982) 807–811.
[10] H. Niedermeyer et al., Max-Planck-Institut fur Plasmaphysik, Garching Rep. IPP-III/90 (1983).
[11] B. Lipschultz et al., Nucl. Fusion 24 (1984) 977.
[12] F. Alladio et al., Phys. Lett. 90A (1982) 405.
[13] J. O'Rourke et al., in: Proc. 12th European Conf. on Controlled Fusion and Plasma Physics, Budapest, Hungary, 1985, contributed papers, Part I, p. 155.
[14] H. Niedermeyer et al., In: Proc. 12th European Conf. on

Controlled Fusion and Plasma Physics, Budapest, Hungary, 1985, contributed papers, Part 1, p. 159.
[15] T.E. Stringer, in: Proc. 12th European Conf. on Controlled Fusion and Plasma Physics, Budapest, Hungary, 1985, contributed papers, Part I, P. 86.
[16] J. Neuhauser, W. Schneider and R.O. Wunderlick, Max-Planck-Institut fur Plasma-physik, Garching Rep#IPP 5/8.
[17] F.P. Boody et al., these Proc. (PSI-VII), J. Nucl. Mater. 145–147 (1987).
[18] P.G. Carolan et al., in: Proc. 12th European Conf. on Cont. Fusion and Plasma Physics, Budapest, Hungary, 1985, contributed papers, Part I, p. 263.
[19] F. Alladio et al., in Plasma Phys. and Cont. Nucl. Fusion Research, 1984, Proc. 10th Int. Conf. London, 1984, Vol I (IAEA, Vienna, 1985) p. 329.
[20] J.D. Strachan et al., in: Proc. 12th Eurpean Conf. on Controlled Fusion and Plasma Physics, Budapest, Hungary, 1985), contributed papers, Part I, p. 339.
[21] J.M. Allen et al., Plasma Phys. Contr. Fusion 28 (1986) 101.
[22] J.D. Strachan et al., these Proc. (PSI-VII), J. Nucl. Mater. 145–147 (1987).
[23] G.M. McCracken et al., these Proc. (PSI-VII), J. Nucl. Mater 145–147 (1987).
[24] K.W. Hill et al., PPPL-2309 March 1986.
[25] P.H. Rebut, R.S. Bickerton and B.E. Keen, Nucl. Fusion 25 (1985) 1011.
[26] R.R. Parker et al. Nucl. Fusion 25 (1985) 1127.
[27] P.G. Carolan and V.A. Piotrowicz, Plasma Phys. 25 (1983) 1065.
[28] B. LaBombard, MIT Plasma Fusion Center Report PFC/RR-86-2.
[29] Y. Shimomura et al., Max-Planck-Institut fur Plasma-physik, Garching, Rep#IPP III/80.
[30] S.J. Kilpatrick et al., J. Vac. Sci. Technol A4 (1986) 1817.
[31] V. Peicoli-Ridolfini, Plasma Phys. Cont. Fusion 27 (1985) 493.
[32] D.K. Owens et al., Bull. Amer. Phys. Soc. 30 (1985) 1520.
[33] B. LaBombard and B. Lipschultz, Rev. Sci. Instr. A4 (1986) 2415.
[34] J. Wesson et al., in: Proc. 12th European Conf. on Controlled Fusion and Plasma Physics, Budapest, Hungary, 1985, Contributed papers, p. 147.
[35] M. Greenwald et al., MIT Plasma Fusion Center Report#PFC/JA-86-22.
[36] J.G. Cordey et al., in: Plasma Physics and Controlled Nuclear Fusion Research, 1984, Proc 10th Int. Conf. London, 1984, Vol. I (IAEA, Verenna, 1985) p. 172.
[37] E.S. Marmar, J. Nucl. Mater. 76 & 77 (1978) 59.